Dynamics of Weak and Strong Collisions: Highly Vibrationally Excited Pyrazine (E = 37900 cm^{-1}) with DCl†

Juan Du, Liwei Yuan, Shizuka Hsieh,‡ Felix Lin, and Amy S. Mullin*

Department of Chemistry and Biochemistry, University of Maryland, College Park, Maryland 20742

Received: March 19, 2008; Revised Manuscript Received: July 17, 2008

The outcome of energy transfer due to single collisions between highly vibrationally excited pyrazine (E = 37900 cm^{-1}) and DCl is measured for the appearance of individual low-J rotational states of DCl using high-resolution transient IR absorption. Appearance profiles from double-Gaussian transient lineshapes were measured for a number of DCl states with $J = 2-12$. These data give information on the recoil velocity distributions, appearance rates, and populations of individual states of the scattered molecules. These data complement previous studies on high-J state DCl scattering (Li, Z.; Korobkova, E.; Werner, K.; Shum, L.; Mullin, A. S. *J. Chem. Phys.* 2005, *123*, 174306), and together, they provide a full description of the V-RT collisions with DCl that quench pyrazine(E). Scattered DCl ($v = 0$) molecules with $J = 2-21$ are rotationally hot with $T_{rot} = 880 \pm 100$ K. Center-of-mass translational energy distributions are $T_{rel} \sim 700$ K for $J < 15$. Broader velocity distributions are observed for the $J = 15-20$ states. The rate constant for V-RT energy transfer is 4.6×10^{-10} cm^3 molecule^{-1} s^{-1}. This value is a lower limit to the overall rate constant for energy transfer and corresponds to ~85% of the Lennard−Jones collision rate. We estimate scattering into the DCl ($v = 1$) state occurs in ~1% of collisions. The energy transfer probability distribution $P(\Delta E)$ is presented and yields $\langle \Delta E \rangle = 888$ cm^{-1}.

Introduction

Collisions that deactivate highly excited molecules compete with reactive processes when they remove enough energy to put the molecule below a critical reaction threshold energy.[1,2] The essence of Hinschelwood's "strong" collision assumption is that deactivation occurs on every collision. In reality, the strength of quenching collisions ranges from nearly elastic processes with small changes in internal energy to impulsive "supercollisions" that exchange large amounts of energy. The strong collision assumption overestimates the effect of collisions on reactivity.[3,4] The importance of collisions that induce small changes in energy has been illustrated in a number of studies on unimolecular reactions.[3,5,6] These studies introduced the term "weak" collisions to account for of the collisions that do not fall into the "strong" collision category. Here, we use the terms "strong" and "weak" as relative descriptors for collisions that induce large and small amounts of energy, respectively. Energy transfer distribution functions obtained from experiments show that weak collisions occur far more often than strong collisions, but dynamical information on weak collisions is difficult to obtain experimentally. By their very nature, weak collisions induce only small changes to the energies and quantum states of the colliding molecules, making it difficult to distinguish their initial and final energy profiles.

We have recently shown that the outcome of weak collisions can be measured by high-resolution transient IR line shape measurements using transitions for low rotational states of the scattered molecules.[7,8] In the work presented here, we report state-resolved experiments that probe the outcome of weak collisions between highly vibrationally excited pyrazine (E = 37900 cm^{-1}) and DCl. In these studies, we have measured the transient appearance of population in low-J states ($J = 2-12$) of DCl that correspond to the products of weak collisions with pyrazine (E). The outcome of strong collisions leading to the appearance of the $J = 15-21$ states of DCl has already been reported. Here, we combine the new low-J data with the earlier high-J data[9] to consider the dynamics of the full range of weak and strong collisions.

A number of experimental approaches have been used to get information about the energy transfer distribution function that describes the collisional relaxation of highly vibrationally excited molecules. A number of these methods detect the highly excited molecules. Barker and co-workers have used time-resolved IR fluorescence (IRF) of photoexcited molecules to monitor collisional relaxation.[10−16] Troe and co-workers have used UV absorption (UVA) to monitor quenching collisions.[17−22] These methods provide information about the average energy transfer for a given donor−bath pair and, in some cases, about the width of the energy transfer distribution function. More recently, Luther and co-workers have used kinetically controlled selective ionization (KCSI) to monitor the appearance of vibrationally excited molecules in well-defined energy windows due to collisional relaxation.[23−27] With knowledge of the initial and final energies of the highly excited molecule, this approach directly yields the energy transfer distribution function. Recently, molecular beam ion imaging has been used to determine the energy transfer distribution functions for highly excited molecules with atomic collision partners.[28−30] Energy transfer distribution functions can also be determined from the perspective of the energy-accepting molecule. Michaels and Flynn developed the formalism for converting J-specific energy gain distributions and rate constants into a probability distribution function.[31] Partial distribution functions from IR studies on strong collisions have been presented for a number of donor−acceptor pairs.[32−36] If state-resolved energy gain data

† Part of the "Stephen R. Leone Festschrift".

* To whom correspondence should be addressed. E-mail: mullin@umd.edu.

‡ Permanent address: Department of Chemistry, Smith College, Northampton, MA 01063.

10.1021/jp802421f CCC: $40.75
Published on Web 08/27/2008

are available for the full distribution of scattered molecules, the complete energy transfer distribution is obtained. For the pyrazine (E)−DCl system, the complete data set for DCl product appearance is used to obtain the full energy transfer probability distribution function.

One important aspect of high-resolution IR energy transfer measurements is that absolute rate constants for specific energy transfer pathways can be determined. Earlier high-resolution studies for a variety of donor (E)/bath collision systems measured the dynamics and rates for strong collisional energy transfer, but because weak collisions were not examined, the reported rates only accounted for one part of the energy transfer distribution.[32−40] Having measurements on the weak collisions allow us to determine the rate constant for energy transfer that occurs through a specific pathway. In this case, we focus on vibration-to-rotation/translation (V-RT) energy transfer, which is the primary relaxation pathway for collisions of highly excited aromatic donors with molecular baths. The rate constant for V-RT energy transfer is the lower limit to the inelastic collision rate. Data of this type are extremely useful in testing the quality of model potentials that are commonly used to describe molecular collisions, such as the Lennard−Jones potentials, and in establishing guidelines for combining parameters in collision systems that can have hydrogen-bonding interactions.[41]

In this paper, we report on the rotational and translational energy gain profiles of DCl ($v = 0$) molecules in low-J states that are populated by collisions with vibrationally excited pyrazine ($E = 37900$ cm^{-1}). High-resolution transient IR absorption line profile measurements are used to distinguish the appearance of collision products from the background thermal population at 300 K. Combined with earlier high-J data, the complete range of weak and strong collisions is characterized. We find that the low-J states have recoil velocity distributions near $T_{rel} = 700$ K for the $J = 2-15$ states of DCl. The average recoil velocities increase for higher J-states of DCl. A single rotational distribution with $T_{rot} = 880$ K describes the scattered DCl ($v = 0$) molecules with $2 < J < 21$. The scattered DCl ($v = 0$) molecules have an appearance rate constant that is ∼85% of the Lennard−Jones collision rate. A small amount of population in DCl ($v = 1$) is observed as a collision product with an estimated energy transfer rate that is a few percent of the Lennard−Jones collisions rate. The energy transfer probability distribution function based on these data is reported. The results are compared with Lennard−Jones collision rates and average energy transfer values from the literature.

Experimental Section

Energy gain measurements in scattered DCl molecules were performed on a high-resolution transient IR laser absorption spectrometer that has been discussed previously.[9] Here, we outline the specifics that apply to this study. A 1:1 gas mixture of DCl and pyrazine flowed through a 3 m collision cell at a total pressure of ∼20 mTorr. Highly vibrationally excited pyrazine was prepared by absorption of 266 nm light from a Nd:YAG laser with a pulse width of 5−7 ns. Radiationless decay to high vibrational levels in the S_0 state occurs with near unity quantum yield in ∼50 ns.[42,43] The UV power density was kept below 1.7 MW/cm^2 to minimize multiphoton absorption. Less than 15% of pyrazine molecules were excited by the UV light. Energy gain in individual DCl ($v = 0$) rotational states was measured by transient IR absorption of DCl ($v = 0, J$) → DCl ($v = 1, J + 1$) R-branch transitions. The appearance of scattered DCl molecules in the ($v = 1$) state was measured with DCl ($v = 1, J$) → DCl ($v = 2, J + 1$) R-branch transitions. The IR probe was a liquid nitrogen-cooled cw IR diode laser operating at $\lambda = 4.3$ μm with a spectral resolution of $\Delta\nu_{IR} = 0.0003$ cm^{-1}.

TABLE 1: IR Probe Transitions for Several Low-J States of DCl

DCl ($v = 0, J$) + hν ($\lambda \sim 4.3$ μm) → DCl ($v = 1, J + 1$)				
J	Cl isotope	ν_0 (cm^{-1})[a]	E_{rot} (cm^{-1})[b]	S_J (cm molecule^{-1})[c]
2	37	2118.960	32.2539	5.2784×10^{-20}
3	37	2128.798	64.4979	5.9385×10^{-20}
4	35	2141.540	107.7895	1.8220×10^{-19}
5	37	2147.758	161.1696	5.4257×10^{-20}
7	35	2168.961	301.5287	1.0940×10^{-19}
12	35	2209.614	837.7971	1.2330×10^{-20}

[a] Line-center absorption frequency ν_0 in cm^{-1} from ref 45. [b] Energy in cm^{-1} of DCl ($v = 0$) rotational states determined using the equation:

$$E_{rot} = B_0[J(J+1)] - D_0[J(J+1)]^2 + H_0[J(J+1)]^3 + L_0[J(J+1)]^4$$

For the D^{35}Cl isotope, $B_0 = 5.39227196(40)$ cm^{-1}, $D_0 = 1.39955(3) \times 10^{-4}$ cm^{-1}, $H_0 = 2.282(8) \times 10^{-9}$ cm^{-1}, and $L_0 = -5.8(5) \times 10^{-14}$ cm^{-1}. For the D^{37}Cl isotope, $B_0 = 5.3764904(2)$ cm^{-1}, $D_0 = 1.31341(21) \times 10^{-4}$ cm^{-1}, $H_0 = 2.2646(65) \times 10^{-9}$ cm^{-1}, and $L_0 = -6.0(5) \times 10^{-14}$ cm^{-1}, from ref 45. [c] Absorption line strength S_J in cm molecule^{-1}. The line strength S_{ji} is the absorption from a lower state j to an upper state i. The line strength S_{ji} is related to the Einstein coefficient B_{ji} for spontaneous emission by the expression

$$S_{ji} = \frac{8\pi^3}{3hc} \cdot \nu_0 \cdot \frac{I_a g_i e^{(-E_j/kT)}}{Q} \cdot (1 - e^{(-\nu_0/kT)}) \cdot \frac{3h^2}{8\pi^3} B_{ji}$$

from ref 44. Here, I_a is the isotopic abundance (0.754 for D^{35}Cl and 0.246 for D^{37}Cl), g_i is the degeneracy of the upper state; E_j is the energy of the lower state; c is the speed of light; and Q is the partition function. The Einstein B_{ji} coefficient is related to the A_{ij} coefficient spontaneous emission by

$$B_{ji} = \frac{g_i}{g_j} \cdot \frac{A_{ij}\lambda^3}{8\pi h}$$

Values for the A_{ij} were determined by Setser and co-workers.[46]

The IR beam was propagated through the cell colinearly with the UV pulse. Transient absorption signals were collected with an InSb detector, amplified, averaged on a digital oscilloscope, and transferred to a computer. The average time between collisions in the pyrazine/DCl mixture was $\tau_{col} \approx 4$ μs. In this study, nascent DCl populations resulting from single collisions with hot pyrazine were determined at $t = 1$ μs after the UV pulse using the DCl spectral information listed in Table 1.[44−46]

Nascent Doppler-broadened line profiles for a number of DCl rotational states with $J = 2-12$ were obtained by collecting transient absorption signals as a function of IR wavelength. Approximately 10% of the IR light passed through a scanning Fabry−Perot etalon and was collected with a second InSb detector. The amplified signal was sent to a lock-in amplifier, which corrected for drifts in the diode laser current so that the IR output was maintained at the center of an etalon fringe. Transient signals were collected at roughly 40 frequency increments across a given line profile.

Pyrazine (Aldrich, 99%+) was purified by freeze−pump−thawing before use. DCl (Cambridge Isotope Laboratories, chemical purity 98% and deuterium purity 99%) was used directly without purification. The DCl sample contained the natural abundance (3:1 ratio) of Cl isotopes (^{35}Cl:^{37}Cl).

Results and Discussion

We report on the energy gain profiles for DCl ($v = 0$) molecules that are scattered in the $J = 2-12$ states due to

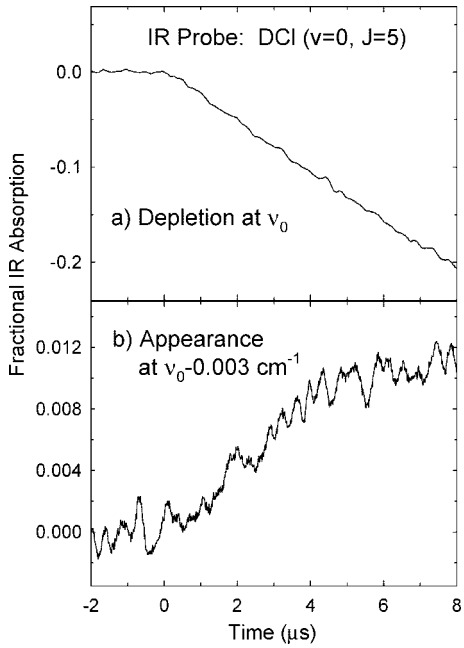

Figure 1. Transient absorption signals for the $J = 5$ state of DCl collisions due to collisions with highly vibrationally excited pyrazine ($E = 37900$ cm^{-1}) at two different IR frequencies. Panel a shows depletion of the initial population at line center ν_0. In panel b, the IR probe is tuned to the wings of the absorption profile at frequency $\nu_0 - 0.003$ cm^{-1}. Here, the appearance of DCl molecules that are products of collisional energy transfer is observed.

collisions with vibrationally excited pyrazine ($E = 37900$ cm^{-1}). Doppler-broadened line profiles based on high-resolution transient IR absorption measurements yield nascent J-specific velocity distributions, populations, and energy transfer rates. Results are combined with earlier data on the $J = 15-21$ states of DCl to consider the full distribution of collisional energy transfer.[9] In the following sections, we present and discuss the translational and rotational energy profiles of the scattered DCl molecules in the $v = 0$ state, the energy transfer rate constant for the V-RT pathway, its connection to the collision rate, and the full energy transfer distribution function for V-RT collisions between pyrazine (E) and DCl. We also report on the observation of collisions that lead to vibrationally excited DCl ($v = 1$) molecules.

Transient Line Profiles of Scattered DCl Molecules in ($v = 0$) and ($v = 1$). To measure the outcome of weak collisions using state-resolved IR probing, it is necessary to distinguish the ambient background from molecules that are scattered in the low-J states. In our experiments, we see appreciable static absorption for the $J = 2-7$ states of DCl ($v = 0$) at 300 K. When highly vibrationally excited pyrazine is generated with 266 nm pulsed light, the transient absorption of these low-J states contains two components. At line center ν_0 of a low-J transition, depletion of the initial DCl population is observed as the molecules in this state undergo collisions with pyrazine (E). In Figure 1a, the negative-going signal represents depletion of the DCl $J = 5$ population at ν_0. The second component corresponds to appearance of collision products. This component is found in the Doppler-broadened wings. In Figure 1b, the IR laser frequency is tuned 0.003 cm^{-1} away from the transition center where a positive-going absorption signal indicates the appearance of DCl molecules in the $J = 5$ state that result from collisions with pyrazine (E).

We have also measured transient IR absorption that corresponds to appearance of the DCl ($v = 1$) state from collisions

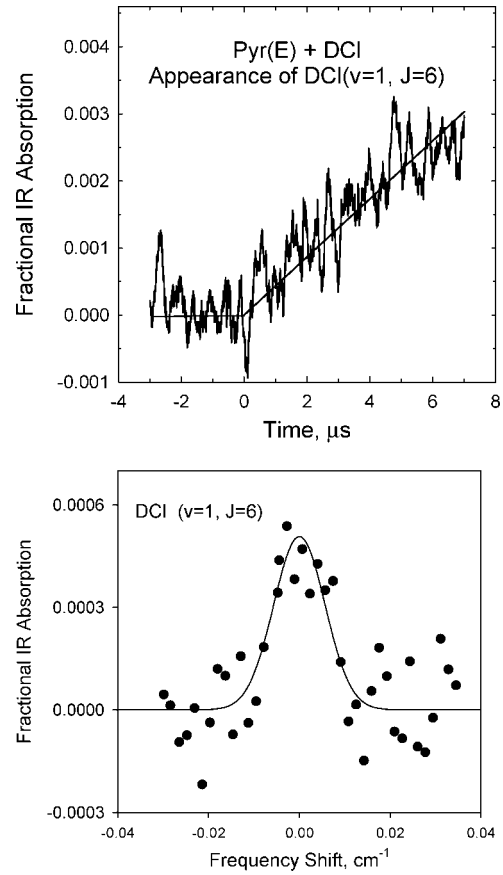

Figure 2. (a) Transient IR absorption of appearance of DCl($v = 1$, $J = 6$) that results from collisions of pyrazine (E) and DCl ($v = 0$), collected at the transition center. (b) Transient absorption line profile for the $J = 6$ state of DCl ($v = 1$) measured 1 μs after the UV excitation of pyrazine.

of pyrazine (E) with DCl ($v = 0$). Linear absorption is directly proportional to the population difference between the lower and the upper states, so measurements of DCl ($v = 0$) are affected by any population in the DCl ($v = 1$) state. At 300 K, the DCl ($v = 1$) population cannot be detected in our experiments, but DCl molecules in the ($v = 1$) state are formed in small amounts through collisions with pyrazine (E). The transient signal for appearance of DCl in the ($v = 1$, $J = 6$) state is shown in Figure 2a. The ($v = 1$, $J = 6$) state is the upper state of the probe transition shown in Figure 1a,b (i.e., the R5 transition of the $v = 1$ state). Figure 2b shows the Doppler-broadened line profile for the ($v = 1$, $J = 6$) state measured at $t = 1$ μs following the UV excitation of pyrazine. This transition is broadened with a full width half-maximum that corresponds to a translational temperature of $T \sim 2000$ K, suggesting that vibrational energy gain in DCl occurs through impulsive collisions. The population of scattered DCl molecules in the ($v = 1$, $J = 6$) state is less than 1% of transient population in the ($v = 0$, $J = 5$) state and has negligible impact on the transient signals for DCl ($v = 0$). With our current experimental set up, signal levels for the DCl ($v = 1$) state are inadequate for characterizing the full distribution of rotational states associated with energy gain the ($v = 1$) state.

Transient absorption signals for the DCl ($v = 0$) state (such as in Figure 1a,b) are linear for the first few microseconds, corresponding to population changes caused by single collisions between DCl and pyrazine (E). IR intensities at $t = 1$ μs describe the nascent DCl populations. Doppler-broadened line profiles at $t = 1$ μs were measured for individual rotational states of

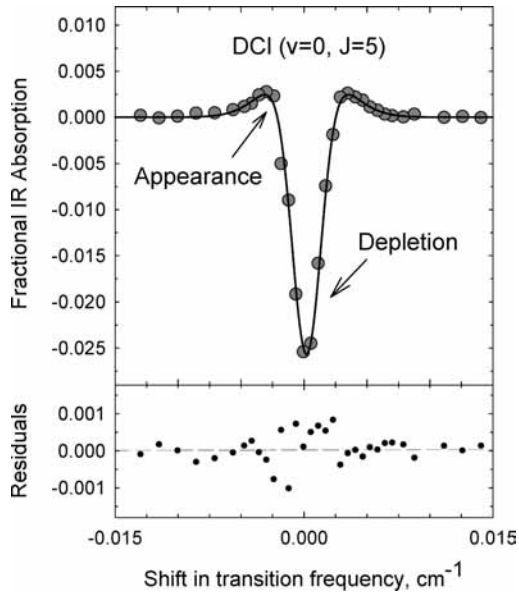

Figure 3. (a) Transient absorption line profile for the $J = 5$ state of DCl ($v = 0$) measured 1 μs after the UV excitation of pyrazine. Open circles are transient IR absorption, and the solid line is the result of fitting with a double-Gaussian function to account for both appearance and depletion of population. (b) Residuals of the fit are shown as solid circles.

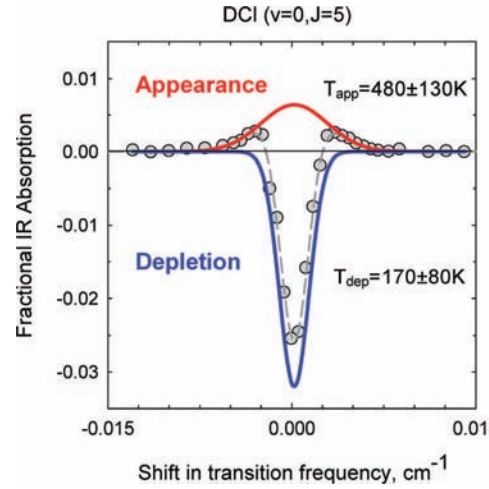

Figure 4. Separate appearance and depletion components of the transient line profile for DCl ($v = 0$) $J = 5$. The filled circles are transient IR data, and the dashed line is the double-Gaussian fitting curve. The appearance component (red line) is broadened due to collisions, with a line width that corresponds to a translational temperature of $T_{app} = 480 \pm 130$ K. The depletion component (blue line) is caused by population loss of the $J = 5$ state and has a translational temperature of $T_{dep} = 170 \pm 80$ K.

DCl. Figure 3 shows the transient line profile for the $J = 5$ state. Depletion of population dominates the profile at line center, while appearance of scattered DCl molecules is seen in the wings of the profile.

The transient line profiles such as shown in Figure 3 are fit to a six-parameter double-Gaussian function using nonlinear least-squares analysis to account for both appearance and depletion components (see Table 2 footnotes). Unique fitting results were obtained for all transitions without external constraints. The result of the fit for the ($v = 0$, $J = 5$) state is shown in Figure 3 as a solid line, and the residuals are shown in the lower section of Figure 3. The fitting procedure yields intensity and line width parameters for the appearance and depletion components. In Figure 4, the appearance component is shown in red and that for depletion is shown in blue. The integrated area under the red appearance curve corresponds to the total population of DCl ($v = 0$) molecules that have scattered into the $J = 5$ state at $t = 1$ μs. Similar curves were obtained for each J state investigated. The distribution of recoil velocities in our measurements is expected to be isotropic (with Gaussian line shapes) since collisions do not occur preferentially along a particular laboratory axis. To check for this, we have performed a series of polarization-dependent studies and verified that transient line profiles are invariant to the polarization and crossing orientation of the UV and IR beams.

Energy Profiles of Scattered DCl ($v = 0$) Molecules. Line widths for appearance $\Delta\nu_{app}$ describe the nascent velocity distributions of the scattered DCl molecules in the $J = 2-12$ states and correspond to laboratory frame translational temperatures of $T_{app} = 480-640$ K. Values of line widths and translational temperatures are listed in Table 2.

The line widths for depletion $\Delta\nu_{dep}$ describe the velocity distribution of the DCl molecules prior to collisions with pyrazine (E). The observed depletion line widths are narrower than 300 K line widths, indicating that collisions of pyrazine (E) with DCl preferentially involve a subset of slower molecules. This result is somewhat surprising given that molecules with higher relative velocities have higher collision rates. In other studies, we have found that collisions of pyrazine (E) with other bath molecules (HOD and CO_2) have depletion line widths that correspond to 300 K velocity distributions.[7,8,47] There is some precedent however for collision cross-sections to increase as a function of decreasing velocity. A negative velocity dependence on collision cross-section has been observed in collisions of Li_2 ($v = 1$) with Xe, Ar, and Ne that lead to quasi-resonant vibration to rotation energy transfer.[48] It is also known that in cases where collisions are dominated by attractive interactions (such as in thermal atomic beams), the collision cross-section is inversely proportional to the relative velocity. For a purely attractive potential where $V(r) = -C/r^6$, the velocity-dependent collision cross-section $\sigma(v)$ is proportional to $v^{-2/5}$ and a negative temperature dependence is observed.[49] It is not entirely clear why pyrazine (E)−DCl collisions have low initial velocities, while HOD and CO_2 show no such preference.

The distributions of recoil velocities are described by the center-of-mass frame translational temperatures T_{rel}. We find that the distributions of relative recoil velocities for the $J = 2-12$ states of DCl have values of $T_{rel} = 570-800$ K. These values are listed in Table 2 and shown in Figure 5 along with earlier high-J results. The recoil velocity distributions for the low-J data are scattered about $T_{rel} \sim 700$ cm^{-1} until $J \sim 15$. For $J > 15$, the translational energy distributions broaden substantially.

Impulsive collisions to bath molecules can impart large changes in both angular momentum and recoil velocity. Figure 5 shows that in collisions of pyrazine (E) with DCl, a threshold for the onset of increasing recoil velocities occurs near $J = 15$. The correlation of angular momentum changes, and recoil velocity is consistent with the Angular Momentum Model by McCaffery and co-workers.[50−53] In Table 3, we compare the average change in recoil velocity of the scattered DCl molecules with average changes in angular momentum, based on an initial $J = 5$ state at 300 K. A discussion of how the angular momentum changes were determined has been presented elsewhere.[9] We find that pyrazine (E)−DCl collisions with $\langle\Delta J_{bath}\rangle = 0-16$ correspond to changes in recoil velocity of $\langle\Delta v_{rel}\rangle \sim 300$ ms^{-1}. For the highest angular momentum changes

TABLE 2: Nascent Doppler-Broadened Line Widths and Translational Temperatures for Low J States of DCl That Are Populated/Depopulated through Collisions with Vibrationally Excited Pyrazine ($E = 37900$ cm^{-1})

	appearance of scattered DCl ($v = 0$, J)			depletion of initial DCl ($v = 0$, J)	
J state	$\Delta\nu_{app}$ (cm^{-1})[a]	T_{app} (K)[b]	T_{rel} (K)[c]	$\Delta\nu_{dep}$ (cm^{-1})[a]	T_{dep} (K)[d]
2	0.0058	570 ± 140	710 ± 170	0.0034	200 ± 100
3	0.0054	490 ± 130	590 ± 150	0.0028	140 ± 80
4	0.0064	640 ± 140	800 ± 180	0.0031	150 ± 80
5	0.0054	480 ± 130	570 ± 150	0.0033	170 ± 100
7	0.0064	620 ± 140	770 ± 170	0.0033	170 ± 100
12	0.0060	520 ± 120	630 ± 150		

[a] Full width at half-maximum (FWHM) line widths $\Delta\nu_{app}$ and $\Delta\nu_{dep}$ for appearance and depletion components, respectively, of individual states of DCl ($v = 0$) measured 1 μs after UV excitation of pyrazine. Line widths are reported to ± 0.001 cm^{-1}. A six-parameter double-Gaussian function $F(\nu)$ is used to fit each line profile using nonlinear least-squares analysis with no constraints:

$$F(\nu) = F_0 + I_{app} \cdot \exp\left[-4 \ln 2 \frac{(\nu - \nu_0)^2}{\Delta\nu_{app}^2}\right] - I_{dep} \cdot \exp\left[-4 \ln 2 \frac{(\nu - \nu_0)^2}{\Delta\nu_{dep}^2}\right]$$

where F_0 is a baseline offset; ν_0 is the center absorption frequency; I_{app} and $\Delta\nu_{app}$ are the intensity and line width for the appearance of product DCl molecules; and I_{dep} and $\Delta\nu_{dep}$ are the intensity and line width that correspond to the depletion of initially populated DCl states. [b] The lab-frame translational temperatures for appearance (T_{app}) and depletion (T_{dep}) are determined from line widths using $T_{lab} = [mc^2/(8R \ln 2)](\Delta\nu_{obs}/\nu_0)^2$, where m is the mass of DCl, c is the speed of light, R is the gas constant, the full width at half-maximum width $\Delta\nu_{obs}$ is $\Delta\nu_{app}$ for appearance and $\Delta\nu_{dep}$ for depletion, and ν_0 is the center frequency of the absorption line. [c] T_{rel} in K, the center-of-mass frame translational temperature for the appearance of scattered DCl, is determined for an isotropic distribution: $T_{rel} = T_{lab} + (m_{DCl}/m_{pyr})(T_{lab} - T_0)$,where m_{DCl} and m_{pyr} are the masses of DCl and pyrazine, respectively, and $T_0 = 300$ K. [d] The translational temperatures based on depletion line widths for initial DCl states.

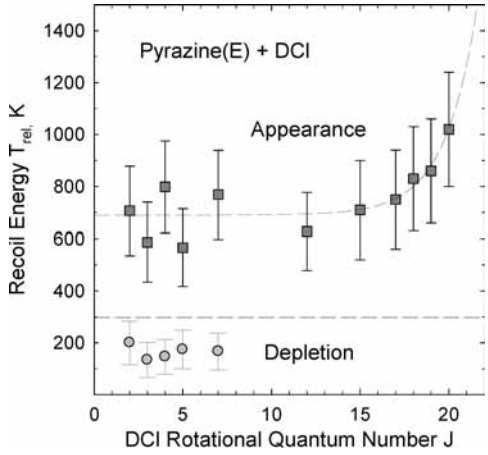

Figure 5. Rotational state dependence of the nascent center-of-mass translational temperatures for pyrazine/DCl collisions. Solid squares show the translational temperatures for the appearance of DCl states with $J = 2-20$ due to collisions with highly vibrationally excited pyrazine ($E = 37900$ cm^{-1}). Data for the $J = 15-20$ states are from ref 9. Open circles are laboratory-frame temperatures for depletion of DCl via collision with hot pyrazine.

that we observe of $\langle\Delta J_{bath}\rangle = 17-19$, the changes in recoil velocity increase to as much as $\langle\Delta v_{rel}\rangle \sim 450$ ms^{-1}.

TABLE 3: Angular Momentum and Recoil Velocities for Individual States of DCl $J = 2-20$ Due to Collisions with Highly Vibrationally Excited Pyrazine ($E = 37900$ cm^{-1})

final J state	$\langle\Delta J_{bath}\rangle$[a]	$\Delta\nu_{app}$[b]	$\langle v_{lab}\rangle$[c]	$\langle v_{rel}\rangle$[d]	$\langle\Delta v_{rel}\rangle$[e]
2	4.6	0.0058	603	817	285
3	4.0	0.0054	559	744	212
4	3.0	0.0064	659	890	348
5	0	0.0054	554	736	203
7	4.9	0.0064	650	877	335
12	10.9	0.0060	600	800	254
15[f]	14.1	0.0063	619	828	286
16	15.2	0.0064	627	840	298
17	16.2	0.0065	635	853	311
18	17.3	0.0068	663	897	355
19	18.3	0.0069	671	910	368
20	19.4	0.0075	728	998	456

[a] The average angular momentum changes $\langle\Delta J_{bath}\rangle$ in units of $\hbar$ of DCl after collisions with vibrationally excited pyrazine are estimated using $\langle\Delta J_{bath}\rangle^2 = |\langle J_{bath}'\rangle^2 - \langle J_{bath}\rangle^2|$. $\langle J_{bath}'\rangle$ is the average final angular momentum vector of DCl determined. The average initial angular momentum vector of DCl at 300 K is $\langle J_{bath}\rangle \sim 5$. [b] FWHM appearance line widths $\Delta\nu_{app}$ in cm^{-1} for DCl($v = 0$) as described in Table 2. [c] The average lab-frame velocity in m (s^{-1}) of individual DCl states following collisions with vibrationally excited pyrazine, determined from $\langle v_{lab}\rangle = (3k_BT_{app}/m_{DCl})^{1/2}$, where k_B is the Boltzmann constant, T_{app} is listed in Table 2, and m_{DCl} is the mass of DCl. [d] The average center-of-mass frame velocity $\langle v_{rel}\rangle$ in m (s^{-1}) for scattered pyrazine and DCl molecules, determined by $\langle v_{rel}\rangle = (M/m_{pyz}) \cdot [\langle v_{lab}\rangle^2 - (3k_BT/M)]^{1/2}$, where M is the total mass of pyrazine and DCl, m_{pyz} is the mass of pyrazine, and $T = 300$ K. [e] The average change in relative velocity $\langle\Delta v_{rel}\rangle$ in m (s^{-1}), determined from $\langle\Delta v_{rel}\rangle = \langle v_{rel}\rangle - (3k_BT/\mu)^{1/2}$, where μ is the reduced mass for DCl + pyrazine collisions. [f] Data for the $J = 15-20$ states are for the D^{35}Cl isotope and are taken from ref 9.

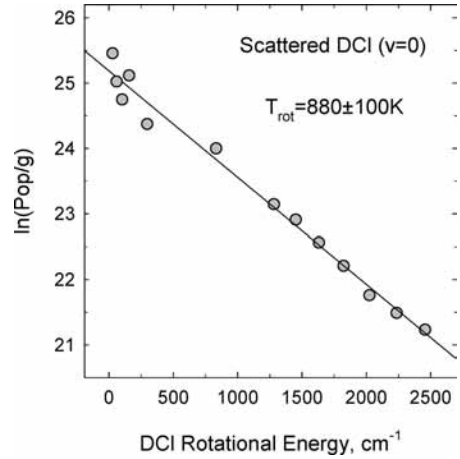

Figure 6. Nascent rotational distribution for the $J = 2-21$ states of DCl that are populated through collisions with vibrationally excited pyrazine. Data for the $J = 15-20$ states are from ref 9. The appearance of DCl molecules due to weak and strong collisions is described by a single Boltzmann distribution with $T_{rot} = 880 \pm 100$ K.

In other experiments, a correlation between angular momentum and recoil velocity is also observed in collisions of pyrazine ($E = 38000$ cm^{-1}) with CO_2, but in this case, values of $\langle\Delta J\rangle$ and $\langle\Delta v_{rel}\rangle$ are substantially greater than when DCl is the bath molecule. Scattered CO_2 molecules are observed in high angular momentum states with $J = 60-80$ with average velocity changes of $\langle\Delta v_{rel}\rangle \sim 1200-2200$ ms^{-1}, respectively.[33,37] Rotational states of CO_2 with $J = 60-80$ have comparable amounts of energy ($E_{rot} = 1442$ and 2553 cm^{-1}, respectively) as DCl states with $J = 16-20$ ($E_{rot} = 1452$ and 2242 cm^{-1}, respectively), but CO_2 molecules in these high-J states are

TABLE 4: State-Specific Rate Constants for Appearance of DCl Products Due to Collisions of Pyrazine ($E = 38000$ cm^{-1}) + DCl → Pyrazine ($E - \Delta E$) + DCl ($v = 0, J$)

DCl J state	E_{rot} (cm^{-1})	k_{app}^J (10^{-12} cm^3 molecule^{-1} s^{-1})
2	32.2539	26 ± 8
3	64.4979	23 ± 7
4	107.7895	23 ± 7
5	161.1696	40 ± 12
7	301.5287	26 ± 8
12	837.7971	30 ± 9
15[a]	1286.115	19 ± 5
16	1456.389	16 ± 4
17	1636.995	12 ± 3
18	1827.878	8.9 ± 2
19	2028.978	6.0 ± 1
20	2240.233	4.8 ± 1
21	2461.58	3.9 ± 1
$k_{app} = \sum_J k_{app}^J$		$(4.6 \pm 1.4) \times 10^{-10}$ cm^3 molecule^{-1} s^{-1}[b]
k_{LJ}		5.4×10^{-10} cm^3 molecule^{-1} s^{-1}[c]

[a] Rate constants for the $J = 15-21$ states are taken from ref 9. [b] Total appearance rate constant k_{app} for V-RT energy transfer of pyrazine (E) + DCl, obtained by summing over the J-specific appearance rates k_{app}^J. [c] The Lennard−Jones collision rate at 300 K for pyrazine (Pyz)/DCl determined from the following equation: $k_{LJ} = (8k_BT/\pi\mu)^{1/2}\,\Omega^{(2,2)^*}\,\pi\sigma^2$. The collision integral $\Omega^{(2,2)^*}$ is $\Omega^{(2,2)^*} = 1.16145(T^*)^{-0.14874} + 0.52487\exp(-0.7732T^*) + 2.16178\exp(-2.43787T^*)$, where $T^* = T/(\varepsilon/k_B)$.[60] Used were the following parameters: $\sigma_{DCl} = 3.36 \times 10^{-10}$ m (ref 61), $(\varepsilon/k_B)_{DCl} = 328$ K (ref 62), and $\sigma_{Pyz} = 5.35 \times 10^{-10}$ m, $(\varepsilon/k_B)_{Pyz} = 435.5$ K (ref 63).

scattered from pyrazine (E) with much more translational energy. This may be due in part to the larger angular momentum changes that are observed for CO_2 and in part to differences in the mass distributions of DCl and CO_2. The amount of rotational and translational energy in the scattered molecules (as well as the partitioning of this energy) depends in a nontrivial way on the collision dynamics, the anisotropy of the intermolecular potential, and the kinematics of the collisions, so a direct comparison of energy partitioning for CO_2 and DCl is not possible. However, when similar amounts of rotational energy are imparted to bath molecules in collisions, our data show that bath molecules with more closely spaced rotational states (and higher angular momentum) are scattered with larger recoil velocities. The rotational constant for CO_2 ($B = 0.39$ cm^{-1}) is relatively small as compared to that for DCl ($B = 5.4$ cm^{-1}).

No such J-dependent increases in T_{rel} are observed in our studies on collisions of pyrazine (E) with H_2O or HOD.[8] Water has small moments of inertia ($A = 27.9$ cm^{-1}, $B = 14.5$ cm^{-1}, and $C = 9.3$ cm^{-1}), and scattered H_2O molecules are observed with rotational energies up to $E_{rot} = 1800$ cm^{-1} in states with $J = 12$. It is not known whether a threshold to the recoil energy distributions exists for higher J states of water, such as seen for DCl and CO_2. Detection of higher J states of water due to collisions with pyrazine (E) requires better experimental sensitivity than we currently have. If the recoil velocities do increase with the higher J states of water, then the onset occurs at J values higher than $J = 12$. It is possible that the mass distribution of water reduces the likelihood of translational energy gain relative to rotational energy in the scattered molecules. It may also be the case that attractive interactions between pyrazine (E) and water influence the energy gain partitioning between the rotational and the translational degrees of freedom. There is evidence from other measurements in our laboratories that preferential interactions of water with the π- and σ-hydrogen-bonding sites on pyridine (C_5H_5N) may favor rotational energy gain in water over translational energy.[54] Whether these types of interactions play a dominant role in determining energy partitioning from collisions remains to be seen. Additional experiments are planned to address this question. In addition, computer simulations should be useful in clarifying the importance of this phenomenon.

The DCl rotational distribution that results from collisions with pyrazine (E) is determined directly from the nascent populations of the $J = 2-21$ states. A semilog plot of the rotationally resolved populations of scattered DCl ($v = 0$) molecules measured 1 μs following collisions with pyrazine (E) is shown in Figure 6. The scattered molecules are well-described by a single Boltzmann distribution with a rotational temperature of $T_{rot} = 880 \pm 100$ K. This result is in good agreement with our previous analysis that considered only the high-J states.

Energy Transfer Rates: Pyrazine (E) + DCl. State-specific rate constants for energy transfer that populates individual rotational states of DCl ($v = 0$) products were determined from J-specific appearance signals (as shown in Figure 4). The rate constant k_{app}^J describes the rate of appearance of DCl ($v = 0, J$) population that comes from quenching collisions of pyrazine (E), as shown in eq 1.

$$\text{pyrazine } (E) + \text{DCl (300 K)} \xrightarrow{k_{app}^J} \text{pyrazine } (E') + \text{DCl } (v = 0, J) \quad (1)$$

The appearance rate of DCl ($v = 0$, J) is given by eq 2.

$$\frac{d[\text{DCl } (J)]}{dt} = k_{app}^J[\text{DCl}][\text{Pyz } (E)] \quad (2)$$

On the basis of the method of initial rates, the appearance rate constant k_{app}^J is determined using eq 3, where $[\text{DCl}]_0$ and $[\text{Pyr } (E)]_0$ are the concentrations at $t = 0$.

$$k_{app}^J = \frac{\Delta[\text{DCl } (J)]}{\Delta t}\,\frac{1}{[\text{DCl}]_0 \cdot [\text{Pyz } (E)]_0} \quad (3)$$

The absolute rate constant for energy gain into the $J = 3$ state was measured using eq 3, and rate contants for the other rotational states of DCl ($J = 2-12$) were determined using the nascent rotational temperature (Figure 6). Values of k_{app}^J are listed in Table 4 for the $J = 2-21$ states of DCl ($v = 0$). Our current results are in very good agreement with the rates published previously for the $J = 15-21$ states.[9]

The kinetics of the V-RT energy transfer pathway is described by the rate constants listed in Table 4. The total rate constant for V-RT energy transfer based on appearance measurements is obtained by summing over the J states of the scattered DCl molecules as shown in eq 4.

$$k_{app} = \sum_J k_{app}^J = (4.6 \pm 1.4) \times 10^{-10}\ \text{cm}^3\ \text{molecule}^{-1}\ \text{s}^{-1} \quad (4)$$

V-RT energy transfer is just one pathway for inelastic collisions of pyrazine (E) with DCl. The value of k_{app} represents a lower limit to the collision rate constant and is ~85% of the Lennard−Jones collision rate constant ($k_{LJ} = 5.4 \times 10^{-10}$ cm^3 molecule^{-1} s^{-1} at 300 K). As discussed previously, energy gain into the ($v = 1$) state of DCl occurs rarely with a rate that is roughly 1% of the Lennard−Jones collision rate, and it is unlikely that higher vibrational states of DCl are populated by collisions. Therefore, k_{app} is essentially the collision rate constant for pyrazine (E)−DCl collisions and is in reasonably good agreement with the Lennard−Jones collision rate.

TABLE 5: Depletion Rate Constant Measurements for Collisions of Pyrazine ($E = 38000$ cm^{-1}) + DCl ($v = 0$, J) → Pyrazine ($E - \Delta E$) + DCl (v', J') at 300 K

DCl J state	E_{rot} (cm^{-1})	k_{dep} (10^{-10} cm^3 molecule^{-1} s^{-1})
2	32.2539	5.6
3	64.4979	3.6
4	107.7895	4.4
5	161.1696	5.1
7	301.5287	2.1
$\langle k_{dep} \rangle$	$(4.3 \pm 1.5) \times 10^{-10}$ cm^3 molecule^{-1} s^{-1}	
k_{LJ}	5.4×10^{-10} cm^3 molecule^{-1} s^{-1}	

State-resolved population depletion measurements can also be used to get a lower limit to the collision rate. The depletion component of the Doppler-broadened transient line profiles consists of DCl molecules that scatter from pyrazine (E). Collisions between highly excited donor molecules and DCl move population out of low-lying J states of DCl that are populated at 300 K as shown in eq 5 and into a distribution of final J' states that have recoil velocities with component Vel along the IR probe axis.

$$\text{donor } (E) + \text{DCl } (J) \rightarrow \text{donor } (E - \Delta E) + \text{DCl } (J', \text{Vel}) \quad (5)$$

It is not necessary for J and J' to have different values to be measured as a scattering event in our studies. Depletion of population occurs as long as either the velocity component along the IR probe axis or the rotational quantum number changes during collisions. The depletion rate of population in the J state is given in eq 6.

$$\text{rate}_{dep}(J) = -\frac{\text{d[DCl } (J)]}{\text{d}t} = k_{dep} f(J)[\text{DCl}][\text{donor } (E)] \quad (6)$$

In eq 6, $f(J)$ is the fractional population in the J state of DCl at 300 K and k_{dep} is the depletion rate constant. We make the reasonable assumption that at 300 K the collision rate does not depend on J. The total depletion rate is a sum of J-specific depletion rates as given by eq 7.

$$\text{rate}_{dep} = \sum_J \text{rate}_{dep}(J) = \left(\sum_J k_{dep} f(J)[\text{DCl}]\right) \times [\text{donor } (E)] = k_{dep}[\text{DCl}][\text{donor } (E)] \quad (7)$$

We report total depletion rate constants in Table 5 based on measurements of double Gaussian transient line profiles for low J states of DCl. The weighted average of the depletion rate constants is $k_{dep} = (4.3 \pm 1.5) \times 10^{-10}$ cm^3 molecule^{-1} s^{-1}. This is in very good agreement with the total appearance rate constant of $k_{app} = (4.6 \pm 1.4) \times 10^{-10}$ cm^3 molecule^{-1} s^{-1}. The agreement of rates based on depletion and appearance gives us confidence in the consistency of this approach for measuring collision rates experimentally.

The agreement between the observed collision rate and the Lennard−Jones rate for DCl−pyrazine (E) collisions is somewhat surprising. HCl is known to form 1:1 hydrogen-bonded complexes with aromatic molecules.[55−58] Lennard−Jones parameters typically do not account for the effects of hydrogen bonding and often underestimate actual collision rates for molecules that are hydrogen-bonded or have other strong intermolecular interactions. In the case of HOD−pyrazine (E) collisions, we measure a collision rate constant that is ~70% larger than the Lennard−Jones rate constant.[7,8] The energy minima for interactions of benzene−water and benzene−HCl have similar energies (~1100 cm^{-1}) and intermolecular distances (~3 Å).[56,59] If these interactions played an important role in collisions, we might expect the collision rate constants for these two systems to show similar enhancements over the Lennard−Jones estimates. The fact that the Lennard−Jones collision rate for DCl−pyrazine (E) is fairly accurate indicates that hydrogen-bonding forces may not be so important in collisions of these molecules.

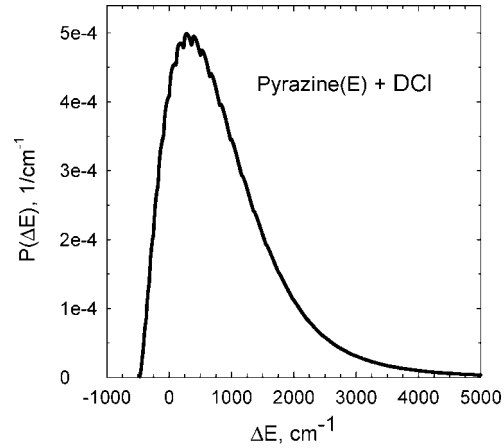

Figure 7. Energy transfer distribution function $P(\Delta E)$ for collisions of vibrationally excited pyrazine ($E = 37900$ cm^{-1}) and DCl as determined from state-resolved appearance measurements. $P(\Delta E)$ is obtained by the adding state-specific energy transfer distributions $P_J(\Delta E)$ for individual J states of DCl, such that $P(\Delta E) = \sum_{\text{all } J} P_J(\Delta E)$.

Full Energy Transfer Distribution Function $P(\Delta E)$. We have characterized the complete distribution of DCl molecules that are scattered from vibrationally hot pyrazine and determined the absolute rate constant for collisions, as described in the preceding section. In this section, we use these results to convert J-indexed energy transfer data into an energy transfer probability distribution that is indexed by ΔE. The state-resolved probability distributions $P_J(\Delta E)$ are determined for each rotational state of DCl based on the Doppler-broadened line widths, the energy transfer rate constants k^J_{app}, and the collision rate.

The full energy transfer probability function $P(\Delta E)$ is the sum of the state-specific $P_J(\Delta E)$ over all DCl rotational states, as shown by eq 8.

$$P(\Delta E) = \sum_{\text{all } J} P_J(\Delta E) \quad (8)$$

The initial rotational and translational energy values for DCl and pyrazine were taken to be the average values at 300 K. Currently, it is not known whether there is any correlation between the initial and final J states of DCl. If such a correlation exists, it is likely that our analysis overestimates the rotational energy changes in DCl. This effect will be most pronounced for weak collisions that lead to small changes in rotational angular momentum. Future experiments that identify the initial J-state of DCl would be useful in addressing this issue.

Figure 7 shows the $P(\Delta E)$ distribution function for energy transfer in collisions of pyrazine (E) and DCl where the probability is referenced to the Lennard−Jones collision rate constant. In the lower plot of Figure 8, the experimental value of the collision rate (k_{app}) has been used to reference the overall probability of the distribution function. The $P(\Delta E)$ curve accounts for all V-RT energy transfer processes that are observed for pyrazine (E)−DCl collisions. The lower $P(\Delta E)$ curve in Figure 8 has an integrated probability of unity.

The relaxation of pyrazine vibrational energy is the driving force for the energy transfer investigated here. The ΔE index

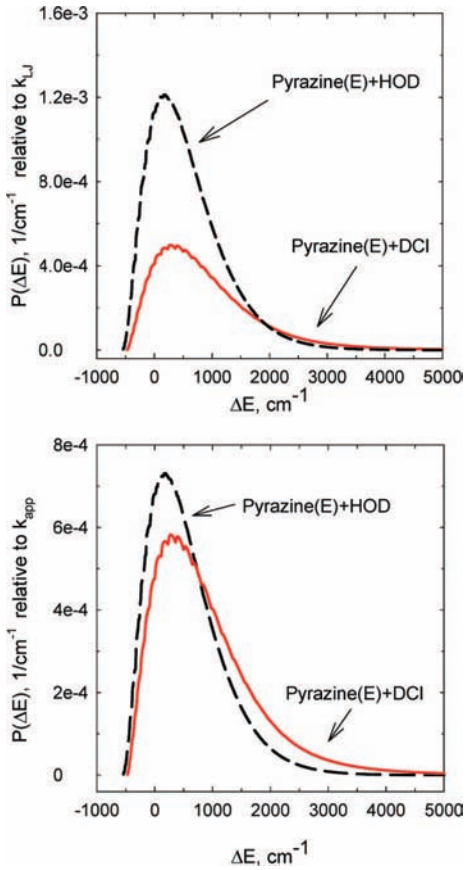

Figure 8. Comparison of the full energy transfer distribution function $P(\Delta E)$ curves for vibrationally excited pyrazine with HOD (taken from ref 8) and DCl (this work). In the upper plot, the energy transfer data are scaled to the Lennard−Jones collision rate. In the lower plot, the energy transfer data are scaled to the measured collision rate.

in $P(\Delta E)$ accounts for pyrazine internal energy that is lost due to collisions with DCl. ΔE includes the rotational energy gain in DCl and the change in recoil energy for DCl and pyrazine (E) based on recoil velocity distribution measurements. It does not account for rotational energy gain in pyrazine (E) that results from collisions with DCl. Our measurements clearly identify how energy is partitioned in the scattered DCl molecules, but we cannot distinguish between the rotational and the vibrational energy content in the scattered pyrazine molecules. We note that $P(\Delta E)$ has a maximum intensity near $\Delta E = 250$ cm^{-1}, which may be related to the distribution of rotational energy that is imparted to pyrazine through collisions with DCl. The $P(\Delta E)$ curve for pyrazine (E)−DCl collisions is dominated by a major feature at positive ΔE values corresponding to energy loss from pyrazine and a smaller feature for negative ΔE values that correspond to collisional energy gain in pyrazine.

On the basis of the data in the lower plot of Figure 8, we determine that the average energy transfer in collisions of pyrazine ($E = 37900$ cm^{-1}) with DCl is $\langle \Delta E \rangle = 888$ cm^{-1}. Barker and Miller have reported average energy transfer values for pyrazine ($E = 3000-33000$ cm^{-1}) with a number of atomic, diatomic, and polyatomic collision partners.[16] However, HCl or DCl is not among the baths studied, so a direct comparison cannot be made with their work. Extrapolating their quenching data to $E = 38000$ cm^{-1} gives the following average energy transfer values: $\langle \Delta E \rangle \sim 50$ cm^{-1} for Ar, ~90 cm^{-1} for CO, ~290 cm^{-1} for CO_2 and CH_4, and ~750 for NH_3 and SF_6. Our value of $\langle \Delta E \rangle = 888$ cm^{-1} for pyrazine/DCl collisions is larger than expected based on their results but is within the same order of magnitude for small polyatomic species.

Comparison with HOD-Pyrazine (E) Collisions. Full energy transfer distribution functions based on state-resolved IR studies have been determined for two collision systems so far. In Figure 8, we compare the $P(\Delta E)$ curves for collisions of pyrazine ($E = 38000$ cm^{-1}) with DCl and with HOD.[8] Figure 8 plots the distribution functions using two different methods for defining the probability. The intensity of $P(\Delta E)$ curves comes directly from the ratio of observed energy transfer rates to the collision rate. In the upper plot, the Lennard−Jones collision rate is used to define the molecular collision rate for each collision pair. In the lower plot, the experimentally determined collision rate is used to normalize each distribution function.

It is apparent from Figure 8 that a comparison of different collision systems depends on the choice of collision rate. From the upper plot, it is clear that water is a more efficient quencher of pyrazine (E) because of the larger area under the HOD curve. Our measurements show that the collision cross-section for pyrazine (E)/HOD at 300 K is $\sigma = 160$ Å^2, while that for DCl with pyrazine is $\sigma = 92$ Å^2. DCl is a larger collision partner than HOD, but HOD has stronger long-range attractive forces that enhance the collision cross-section and are not accounted for in the Lennard−Jones collision model. The fact that the collision rate for DCl−pyrazine is close to the Lennard−Jones rate indicates that long-range interactions are not very important in the collisional energy transfer between these molecules.

It is important to recognize that efficient quenching by water is due in large part to its high collision rate and not from the presence of a prominent large ΔE component in the tail of the distribution function. In fact, the ΔE distribution for HOD is notably narrower than for DCl, as illustrated in the lower plot of Figure 8 where the observed collision rates are used to determine probabilities and the area under each curve is unity. Long-range attractive forces between pyrazine and HOD enhance the cross-section for inelastic collisions by effectively extending the range at which collisions are sufficiently strong to cause some energy transfer to take place but, at the same time, decrease the average energy transfer. In the lower plot, we see that there are more strong collisions for quenching with DCl, which lead to DCl molecules scattered into high rotational states with broad velocity distributions. For HOD, it may be that the additional collisions caused by enhanced long-range attraction lead only to relatively weak energy transfer. It may also be the case that HOD collisions are weaker due to details of the energy transfer involving preferential hydrogen-bonding configurations. There is evidence from other work in our laboratory that the likelihood of large ΔE collisions involving water is affected by preferred geometries of water in collisions with pyridine molecules. While it is unlikely that long-lived complexes form at 300 K, details of the collision dynamics will be sensitive to anisotropy in the intermolecular potential energy surface. One definite conclusion that can be reached from the relatively modest amounts of energy transferred overall and the low probability of forming DCl in the ($v = 1$) state is that long-lived complex formation leading to anything even approaching a full statistical redistribution of energy is extremely rare.

Conclusion

The ability to measure state-resolved energy gain profiles for weak collisions is opening up exciting opportunities for understanding the collision dynamics of highly excited molecules. Detailed information about weak collisions and their energy transfer properties complements earlier studies on strong collisions and allows us to profile the entire distribution of energy transfer events from a quantum-

resolved perspective. These studies also provide a direct measurement of the collision rate. Comparison of experimental collision rates and Lennard−Jones rates clarifies the role of hydrogen bonding and other specific interactions in energy transfer collisions. We find that DCl−pyrazine (E) collisions primarily lead to V-RT energy transfer with an integrated rate that is ∼85% of the Lennard−Jones collision rate. Very small amounts of vibrational excitation of DCl in the $v = 1$ state is observed. A threshold for strong collisions is observed for DCl products near the $J = 15$ state where the velocity distributions show J-dependent broadening. The energy transfer distribution function contains evidence of a strong collision component and yields an average energy transfer value of $\langle \Delta E \rangle = 888$ cm^{-1}. Studies of this kind provide important guidelines in developing theoretical models of molecular collisions under high temperature conditions.

Acknowledgment. We gratefully acknowledge research support from the Department of Energy (DE-FG02-06ER15761), with additional equipment support from the National Science Foundation (CHE-0552663) and the University of Maryland.

References and Notes

(1) Baer, T.; Hase, W. L. *Unimolecular Reaction Dynamics*; Oxford University Press: New York, 1996.
(2) Tardy, D. C.; Rabinovitch, B. S. *Chem. Rev.* **1977**, *77*, 369.
(3) Troe, J. *J. Chem. Phys.* **1977**, *66*, 4745.
(4) Troe, J. *J. Chem. Phys.* **1977**, *66*, 4758.
(5) Snavely, D. L.; Zare, R. N.; Miller, J. A.; Chandler, D. W. *J. Phys. Chem.* **1986**, *90*, 3544.
(6) Chan, S. C.; Rabinovitch, B. S.; Bryant, J. T.; Spicer, L. D.; Fujimoto, T.; Lin, Y. N.; Pavlou, S. P. *J. Phys. Chem.* **1970**, *74*, 3160.
(7) Havey, D. K.; Liu, Q.; Li, Z. M.; Elioff, M.; Fang, M.; Neudel, J.; Mullin, A. S. *J. Phys. Chem. A* **2007**, *111*, 2458.
(8) Havey, D. K.; Liu, Q. N.; Li, Z. M.; Elioff, M.; Mullin, A. S. *J. Phys. Chem. A* **2007**, *111*, 13321.
(9) Li, Z.; Korobkova, E.; Werner, K.; Shum, L.; Mullin, A. S. *J. Chem. Phys.* **2005**, *123*, 174306.
(10) Toselli, B. M.; Brenner, J. D.; Yerram, M. L.; Chin, W. E.; King, K. D.; Barker, J. R. *J. Chem. Phys.* **1991**, *95*, 176.
(11) Toselli, B. M.; Barker, J. R. *J. Chem. Phys.* **1991**, *95*, 8108.
(12) Toselli, B. M.; Barker, J. R. *J. Chem. Phys.* **1992**, *97*, 1809.
(13) Barker, J. R. *J. Phys. Chem.* **1984**, *88*, 11.
(14) Barker, J. R.; Toselli, B. M. *Int. Rev. Phys. Chem.* **1993**, *12*, 305.
(15) Miller, L. A.; Cook, C. D.; Barker, J. R. *J. Chem. Phys.* **1996**, *105*, 3012.
(16) Miller, L. A.; Barker, J. R. *J. Chem. Phys.* **1996**, *105*, 1383.
(17) Hippler, H.; Troe, J.; Wendelken, H. J. *Chem. Phys. Lett.* **1981**, *84*, 257.
(18) Hippler, H.; Luther, K.; Troe, J.; Wendelken, H. J. *J. Chem. Phys.* **1983**, *79*, 239.
(19) Hippler, H.; Troe, J.; Wendelken, H. J. *J. Chem. Phys.* **1983**, *78*, 5351.
(20) Hippler, H.; Lindemann, L.; Troe, J. *J. Chem. Phys.* **1985**, *83*, 3906.
(21) Hippler, H.; Otto, B.; Troe, J. *Ber. Bunsen-Ges.* **1989**, *93*, 428.
(22) Heymann, M.; Hippler, H.; Troe, J. *J. Chem. Phys.* **1984**, *80*, 1853.
(23) Grigoleit, U.; Lenzer, T.; Luther, K.; Mutzel, M.; Takahara, A. *Phys. Chem. Chem. Phys.* **2001**, *3*, 2191.
(24) Hold, U.; Lenzer, T.; Luther, K.; Reihs, K.; Symonds, A. C. *J. Chem. Phys.* **2000**, *112*, 4076.
(25) Lenzer, T.; Luther, K.; Reihs, K.; Symonds, A. C. *J. Chem. Phys.* **2000**, *112*, 4090.
(26) Hold, U.; Lenzer, T.; Luther, K.; Symonds, A. C. *J. Chem. Phys.* **2003**, *119*, 11192.
(27) Frerichs, H.; Hollerbach, M.; Lenzer, T.; Luther, K. *J. Phys. Chem. A* **2006**, *110*, 3179.
(28) Liu, C. L.; Hsu, H. C.; Lyu, J. J.; Ni, C. K. *J. Chem. Phys.* **2005**, 123.
(29) Bernshtein, V.; Oref, I.; Liu, C. L.; Hsu, H. C.; Ni, C. K. *Chem. Phys. Lett.* **2006**, *429*, 317.
(30) Liu, C. L.; Hsu, H. C.; Lyu, J. J.; Ni, C. K. *J. Chem. Phys.* **2006**, 125.
(31) Michaels, C. A.; Flynn, G. W. *J. Chem. Phys.* **1997**, *106*, 3558.
(32) Wall, M. C.; Stewart, B. A.; Mullin, A. S. *J. Chem. Phys.* **1998**, *108*, 6185.
(33) Wall, M. C.; Mullin, A. S. *J. Chem. Phys.* **1998**, *108*, 9658.
(34) Michaels, C. A.; Lin, Z.; Mullin, A. S.; Tapalian, H. C.; Flynn, G. W. *J. Chem. Phys.* **1997**, *106*, 7055.
(35) Park, J.; Shum, L.; Lemoff, A. S.; Werner, K.; Mullin, A. S. *J. Chem. Phys.* **2002**, *117*, 5221.
(36) Sevy, E. T.; Rubin, S. M.; Lin, Z.; Flynn, G. W. *J. Chem. Phys.* **2000**, *113*, 4912.
(37) Mullin, A. S.; Michaels, C. A.; Flynn, G. W. *J. Chem. Phys.* **1995**, *102*, 6032.
(38) Fraelich, M.; Elioff, M. S.; Mullin, A. S. *J. Phys. Chem. A* **1998**, *102*, 9761.
(39) Elioff, M. S.; Fraelich, M.; Sansom, R. L.; Mullin, A. S. *J. Chem. Phys.* **1999**, *111*, 3517.
(40) Elioff, M. S.; Fang, M.; Mullin, A. S. *J. Chem. Phys.* **2001**, *115*, 6990.
(41) Wormald, C. J.; Wurzberger, B. *Phys. Chem. Chem. Phys.* **2000**, *2*, 5133.
(42) Dietz, T. G.; Duncan, M. A.; Puiu, A. C.; Smalley, R. E. *J. Phys. Chem.* **1982**, *86*, 4026.
(43) Knee, J.; Johnson, P. *J. Phys. Chem.* **1985**, *89*, 948.
(44) Rothman, L. S.; Jacquemart, D.; et al. *J. Quantum Spectrosc. Radiat. Transfer* **2005**, *96*, 139.
(45) Parekunnel, T.; Hirao, T.; Le Roy, R. J.; Bernath, P. F. *J. Mol. Spectrosc.* **1999**, *195*, 185.
(46) Arunan, E.; Setser, D. W.; Ogilvie, J. F. *J. Chem. Phys.* **1992**, *97*, 1734.
(47) Havey, D. K.; Du, J.; Lui, Q.; Mullin, A. S. Manuscript in preparation.
(48) Scott, T. P.; Smith, N.; Magill, P. D.; Pritchard, D. E.; Stewart, B. *J. Phys. Chem.* **1996**, *100*, 7981.
(49) Bernstein, R. B. *J. Chem. Phys.* **1961**, *34*, 361.
(50) McCaffery, A. J.; Osborne, M. A.; Marsh, R. J.; Lawrance, W. D.; Waclawik, E. R. *J. Chem. Phys.* **2004**, *121*, 169.
(51) Clare, S.; Marks, A. J.; McCaffery, A. J. *J. Phys. Chem. A* **2000**, *104*, 7181.
(52) Osborne, M. A.; McCaffery, A. J. *J. Chem. Phys.* **1994**, *101*, 5604.
(53) McCaffery, A. J.; Alwahabi, Z. T.; Osborne, M. A.; Williams, C. J. *J. Chem. Phys.* **1993**, *98*, 4586.
(54) Liu, Q.; Havey, D. K.; Mullin, A. S. *J. Phys. Chem. A* **2008**, *112*, 9509.
(55) Gotch, A. J.; Zwier, T. S. *J. Chem. Phys.* **1990**, *93*, 6977.
(56) Cheney, B. V.; Schulz, M. W.; Cheney, J.; Richards, W. G. *J. Am. Chem. Soc.* **1988**, *110*, 4195.
(57) Cheney, B. V.; Schulz, M. W. *J. Phys. Chem.* **1990**, *94*, 6268.
(58) Read, W. G.; Campbell, E. J.; Henderson, G.; Flygare, W. H. *J. Am. Chem. Soc.* **1981**, *103*, 7670.
(59) Zhao, Y.; Tishchenko, O.; Truhlar, D. G. *J. Phys. Chem. B* **2005**, *109*, 19046.
(60) Lim, K. F. *Quant. Chem. Prog. Exch.* **1994**, *14*, 3.
(61) Zeleznik, F. J.; Dugan, J. V., Jr. *J. Chem. Phys.* **1971**, *54*, 4523.
(62) Hirschfelder, J. O.; Curtis, C. F.; Bird, R. B. *Molecular Theory of Gases and Liquids*; Wiley: New York, 1964.
(63) Bevilacqua, T. J.; Weisman, R. B. *J. Chem. Phys.* **1993**, *98*, 6316.

JP802421F